COMMUNICATION

ADVANCED
MATERIALS
www.advmat.d

Check for
updates

Liquid-Crystal-Elastomer-Based Dissipative Structures by Digital Light Processing 3D Printing

*Nicholas A. Traugutt, Devesh Mistry, Chaoqian Luo, Kai Yu, Qi Ge,** and Christopher M. Yakacki**

Digital Light Processing (DLP) 3D printing enables the creation of hierarchical complex structures with specific micro- and macroscopic architectures that are impossible to achieve through traditional manufacturing methods. Here, this hierarchy is extended to the mesoscopic length scale for optimized devices that dissipate mechanical energy. A photocurable, thus DLP-printable main-chain liquid crystal elastomer (LCE) resin is reported and used to print a variety of complex, high-resolution energy-dissipative devices. Using compressive mechanical testing, the stress–strain responses of 3D-printed LCE lattice structures are shown to have 12 times greater rate-dependence and up to 27 times greater strain–energy dissipation compared to those printed from a commercially available photocurable elastomer resin. The reported behaviors of these structures provide further insight into the much-overlooked energy-dissipation properties of LCEs and can inspire the development of high-energy-absorbing device applications.

The surge of additive manufacturing technologies is driving the ability to process novel multifunctional materials into precisely controlled architectures—allowing us to readily optimize a device's performance for specific applications.[1,2–4] One key application area is the development of bespoke lattice structures from soft materials for dissipation of mechanical energy. This includes sports and personal protective equipment as well as biomedical devices.[5–7] In this study, we are the first to explore how liquid-crystalline materials with inherent dissipative behavior can be 3D printed to create energy dissipative structures.

Tailoring the geometry of 3D-printed lattices offers control over mechanical and dissipative properties.[5,8,9] For example, one can produce negative Poisson's ratio geometries that are expected to possess enhanced dissipative properties.[10,11] Dissipation can also be increased through design of buckling architectures where elastic energy stored in the deformation of members is dissipated as they snap through to buckled states.[9,10] In the above examples, geometry tunes and dictates the lattices' mechanical properties. Conventional soft materials were chosen for their ease of printing, with less consideration given to the printed material's viscoelasticity—despite the critical importance of viscoelasticity to dissipation of mechanical energy.

Liquid crystal elastomers (LCEs) are soft and multifunctional materials that combine anisotropic molecular order of liquid crystals (LCs) with the entropic elasticity of a lightly cross-linked polymer network.[12,13] These materials are most celebrated for their potential as soft robotic actuators.[14,15] However, LCEs also have exceptional mechanical properties such as high energy dissipation, soft elasticity, programmable anisotropy, negative Poisson's ratios, and nonlinearity—properties reminiscent of soft biological tissues.[16,17] Until recently, LCEs were largely limited to thin-film (<150 μm) devices due to complex synthesis routes and need to align the LC groups via surface effects.[13,18] Recent years have seen the development of click chemistries and direct ink writing (DIW) technologies that now enable the fabrication of macroscopic LCE devices.[15,19–21]

In this study, we develop a new photocurable thiol-acrylate LC resin optimized for Digital Light Processing (DLP) 3D printing—a vat photopolymerization-based process whereby 3D objects are printed through photocuring of successive thin layers of a photopolymer. When cured, this LC resin forms a LC elastomer with highly pronounced dissipative properties at 30 °C above its glass transition temperature (T_g)—a phenomenon not observed in traditional elastomers.

Of the many additive manufacturing technologies available today, vat photopolymerization-based printing is the technology capable of printing large-scale soft material devices (dimensions >10 mm) with high resolution (≈10 μm) and complex features (e.g., overhangs).[2,3,22,23] DLP printing is also a high-throughput and scalable technology, which makes it become an attractive method for the commercial fabrication of architected dissipative lattices.[3,23]

Using DLP printing, we fabricate lattice devices from our LC resin and a commercial resin, TangoBlack (Stratasys Ltd., Eden Prairie, MN, USA), and compare their performance via mechanical testing.[21,24] As illustrated by our design

N. A. Traugutt, Dr. D. Mistry, C. Luo, Prof. K. Yu, Prof. C. M. Yakacki
University of Colorado Denver
1200 Larimer Street, Campus Box 112, Denver, CO 80217, USA
E-mail: chris.yakacki@ucdenver.edu
Prof. Q. Ge
Department of Mechanical and Energy Engineering
Southern University of Science and Technology
1088 Xueyuan Avenue, Shenzhen 518055, P. R. China
E-mail: geq@sustech.edu.cn

The ORCID identification number(s) for the author(s) of this article can be found under https://doi.org/10.1002/adma.202000797.
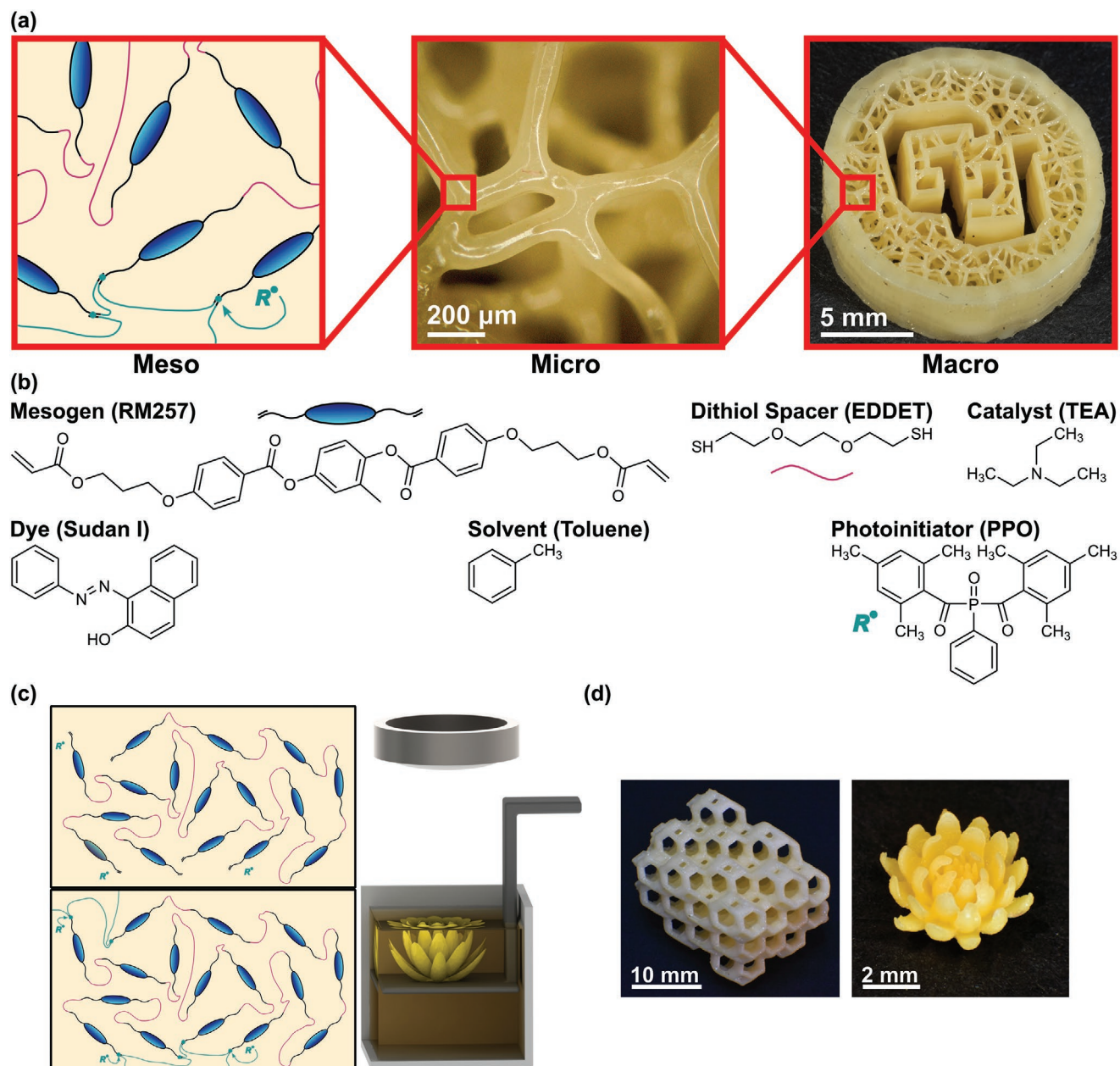
Figure 1. a) Our motivation: dissipation controlled across length scales from the resin chemistry (mesoscale), to the microscale lattice architecture, and the overall macrostructure of printed structures. b) Structures of the chemical monomers and components that form our printable resin. Acrylate-capped oligomer chains of alternating RM257 and EDDET are synthesized via a Michael addition using the catalyst TEA. Photoinitiator PPO allows photocuring of free excess acrylate groups during printing. The dye Sudan I enables micrometer-scale print resolutions. Resin viscosity is lowered using toluene. c) DLP printing project masks of UV light through a magnifying lens to selectively cure each print layer. d) Sample prints of a lattice (left) and lotus flower (right) demonstrate the range print sizes, resolutions, and complexities possible.

paradigm in **Figure 1**a, the DLP-printed LCE lattices have mechanical properties controlled across length scales: on the mesoscale, viscoelasticity is tuned via the LCE chemistry; on the microscale, mechanical behaviors are controlled via isotropic and anisotropic lattice architectures; and lastly, on the macroscale, we specify the overall device geometry. This control of mechanical properties allows complete optimization of a dissipative device—important for applications such as electronic devices or protective equipment where

there is often minimal space available for impact absorbing elements.

Bulk LCE test devices with high resolution details and complex shapes were created using a bespoke thiol-acrylate LC resin (Figure 1b) and a custom DLP 3D printer (Figure 1c). The DLP printer uses a UV light engine to project masked images to photopolymerize the LC resin in a top-down, layer-by-layer process.[25] Two sample prints of a lattice and a lotus flower (Figure 1d) demonstrate the resolution offered by the process.

ADVANCED
SCIENCE NEWS
www.advancedsciencenews.com

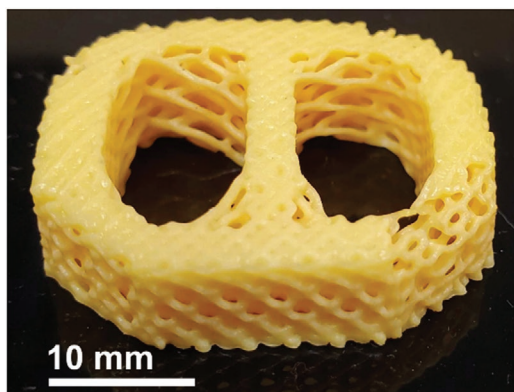ADVANCED
MATERIALS
www.advmat.de

Figure 2. A DLP-printed LCE concept device of a spinal cage with a porous lattice architecture.

The lattice structure was 550 consecutively printed 50 μm layers and measures ≈15.5 × 15.5 mm along its length and width. The lotus flower was printed with 10 μm layer heights and demonstrates the high resolution available with printing. A 33 × 28 × 9 mm³ LCE spinal cage concept device (**Figure 2**) was printed with 100 μm layer heights using an Original Prusa SL1 (Prusa Research, Prague, Czech Republic) to expand on the implications, usefulness, and scalability of our technique.

Photographs of the three different lattice structures with orthotropic (Lattice A), isotropic (Lattice B), and transverse isotropic (Lattice C) symmetries printed from our LC resin are shown in **Figure 3**a. For comparison with a conventional isotropic elastomer network, Lattice A-type structures were printed from TangoBlack. The performance of the structures was compared via compressive testing. A representative stress–strain curve for testing in the x-axis at fastest and slowest strains is shown in Figure 3b. For accurate comparisons between our LCE and TangoBlack, testing on both materials was performed at 28 °C above their respective T_g. This corresponded to room temperature for the LCE samples and 42 °C for TangoBlack samples. The respective T_g values were determined via dynamic mechanical analysis (DMA), which is detailed in the Supporting Information. As the strain rate was increased from 0.21 to 220% s^{-1}, the peak stress for the LCE Lattice A on average was increased by 370% (from 0.054 to 0.207 MPa)—far larger than the 5% increase displayed by the TangoBlack Lattice A (from 0.042 to 0.044 MPa) (Table S1, Supporting Information). Additional stress–strain curves for each structure, strain rate, and direction of loading can be found in Figures S1–S4 (Supporting Information). It was noted that the LCE lattices recovered their shape after 2–5 min at room temperature, depending on the loading and unloading rates. If heated above T_i, the structures would recover immediately. The TangoBlack lattice recovered its shape and dimensions immediately. The residual strain seen in Figure S4 (Supporting Information) is the result of experimental limitations, where the crosshead
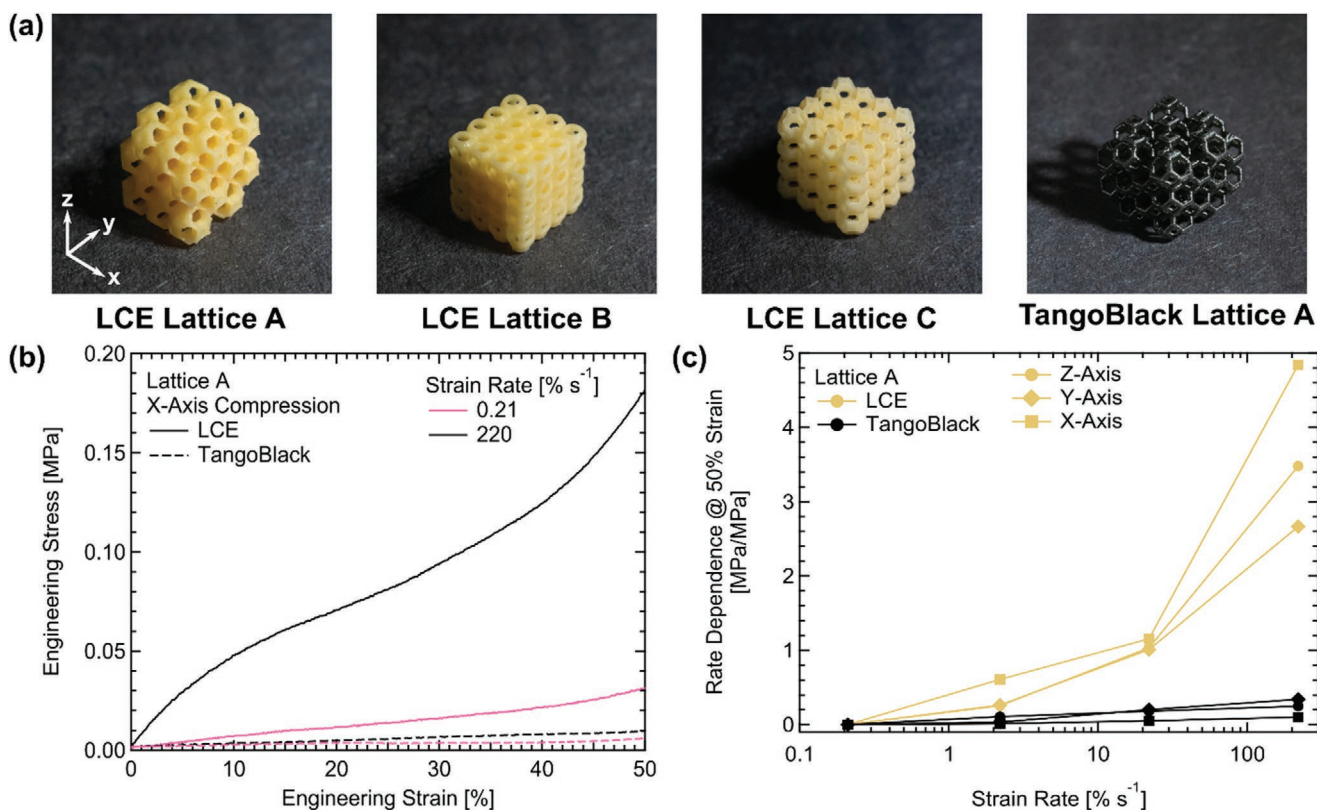

Figure 3. a) Pictures of each DLP-printed lattice are shown. b) DLP 3D-printed LCE and TangoBlack lattices were tested under uniaxial compressive loading and stress responses were observed. c) Stress values at 50% strain for Lattice A were observed to quantify rate-dependence for the two materials. $n = 1$ was used for these tests.
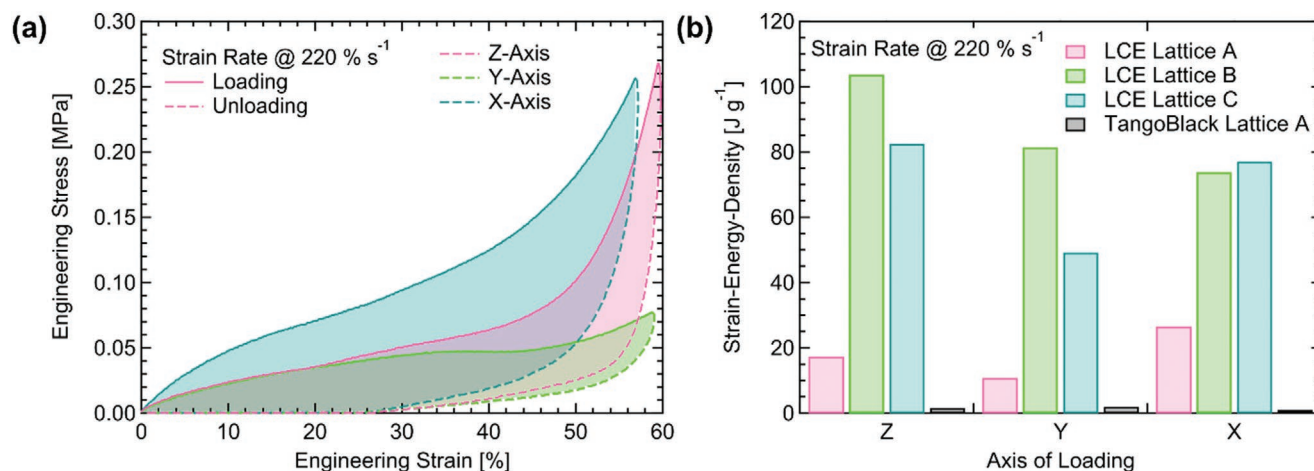
Figure 4. Strain energy density was observed to compare the damping abilities of different lattices made from LCEs. a) Area under the curve was used to calculate strain energy density. b) Comparisons of each lattice are shown. $n = 1$ was used for these tests.

was not decompressing the sample quickly enough to show the elastic response.

For determining the rate-dependence, RD, of each material at each given strain rate, $\dot{\varepsilon}$, we used

$$\text{RD}(\varepsilon) = \frac{\sigma_{\dot{\varepsilon}}(\varepsilon) - \sigma_{\dot{\varepsilon}=\text{quasistatic}}(\varepsilon)}{\sigma_{\dot{\varepsilon}=\text{quasistatic}}(\varepsilon)} \qquad (1)$$

where $\sigma_{\dot{\varepsilon}}$ is the stress at the chosen strain, ε, and strain rate. For our experiments, we measured the stress at the strain of 50%, and used a quasistatic strain rate of 0.21% s^{-1}. On average, the maximum rate-dependency of the LCE was 3.66, which is over 12 times greater than that of the TangoBlack lattice whose rate-dependence was 0.23. We also note that the lattice geometries introduced hyperelastic behavior before it experiences strain stiffening. A summary of the rate-dependent behavior for Lattice A can be seen in Figure 3c.

The strain energy density, a measure of hysteresis and energy loss, for each lattice loading direction and material is shown in **Figure 4**. Dividing this by the overall apparent density of the respective lattice provides a metric allowing us to compare the influence of lattice structure on dissipation. LCE lattices A, B, and C had apparent densities of 0.33, 0.52, and 0.31 g cm^{-3}, respectively. TangoBlack Lattice A had an apparent density of 0.18 g cm^{-3}.

Figure 4a shows a representative plot showing area under the curve for LCE Lattice A compressed at 220% s^{-1} along the x, y, and z axes. Figure 4b compares the strain energy densities of all lattice structures displaced at 220% s^{-1}. The strain energy densities and peak stresses of all lattice structures, for each strain rate and direction of loading, can be found in Table S1 (Supporting Information). Comparing the differences in strain energy densities for the orthotropic Lattice A, we see that the LCE outperforms TangoBlack in all loading directions and at all testing rates. At the slowest (quasistatic) rate, the TangoBlack Lattice demonstrates almost negligible energy dissipation, while the LCE Lattice has energy density values ranging from 3.00 to 4.72 J g^{-1}. At the faster rates, the TangoBlack demonstrated energy loss values from 0.29 to 1.98 J g^{-1}, while the LCE increased to a maximum of 26.62 J g^{-1}. In all of the faster rate

tests, the LCE lattice had a range of 5 to 27 times greater strain energy density than TangoBlack.

While Lattice B has an isotropic symmetry, the strain energy densities along the x, y, and z directions show LCE Lattice B which is transversely isotropic. For example, for loading at 220% s^{-1}, the strain energy density along the z-direction (103.60 J g^{-1}) ≈1.25 times greater than those for loadings along the x or y axes (81.44 and 73.80 J g^{-1}) which are comparatively similar. This breaking of symmetry in a lattice of isotropic symmetry can be explained by the fact that the lattice is printed in a layer-by-layer fashion.

In this study, we explored tailorable energy dissipation in DLP-printed anisotropic and isotropic lattice structures fabricated from a custom photocurable LC resin. Comparing lattices made from our LCE with those made from a commercially available photocurable resin, TangoBlack, the LCE demonstrates over 12 times greater rate-dependency (Figure 3), moderate hysteresis (i.e., energy loss) under quasistatic testing, and up to 27 times greater strain energy density (Figure 4). The greater rate-dependency demonstrated by the LCEs can be explained by the rotation of mesogen and liquid-crystal domains when strained, which adds an additional mechanism of viscous effects in the rubbery regime and was explored in a study by Azoug et al.[26] The increased performance of our LCE can be understood by comparing the bulk thermomechanical properties of our LCE against those of TangoBlack. Our LCE has inherently higher levels of energy dissipation than TangoBlack, as it has elevated tan δ values of around 0.5 when heated 30 °C above its glass transition (Figure S5, Supporting Information). The LCE's elevated tan δ is also significantly higher than that of other traditional elastomers, such as neoprene (a common shock absorber), nitrile and silicone—materials which currently are not DLP-printable (Figure S6, Supporting Information). The two different peaks in the tan δ curve, along with the storage modulus, behavior suggest the neoprene is a copolymer and exhibits two different T_g peaks. After the second T_g peak, the neoprene is fully in the rubbery regime. Moreover, solid cubes of our LCE have more than 140 times greater rate-dependency than solid cubes of TangoBlack (Figure S7, Supporting Information).

**ADVANCED
SCIENCE NEWS**

www.advancedsciencenews.com

**ADVANCED
MATERIALS**

www.advmat.de

The high levels of dissipation and rate-dependence of the LCE material make it attractive for use in a wide range of protective applications, such as protective body equipment (e.g., helmets) and impact absorbers in industrial equipment and electronics. Introducing rate-dependent materials into these applications is particularly interesting as the material can adapt its stiffness to the rate of compression—offering protection under a wider range of impact conditions. In a recent biomechanical analysis of football helmets, Alizadeh et al. discussed how ideal energy-dissipating materials would adjust their properties to maximize the stroke under all impact conditions.[7] Their study showed that under theoretically ideal conditions, concussions may be reduced by 73%.[7] The high rate-dependence and soft-elastic behavior of liquid-crystal materials may provide a means to help approach these ideal impact conditions. When designing personal safety equipment or protective features for machines and electronics, it makes more sense to use a durable material that will be able to maximize energy dissipation while minimizing peak stresses across a range of loading conditions.

The potential range-of-use for this LCE is between T_g and T_i, that is, a 60 °C window (−6 to ≈55 °C), where the tan δ is elevated and the material is nematic (Figure S5, Supporting Information). Conversely, traditional viscoelastic materials are highly temperature-dependent and only exhibit an elevated tan δ near T_g, where their tan δ is also highly temperature-dependent and their modulus approaches gigapascals. DMA and DSC tests measured T_g, T_i, and an elevated tan δ curve between T_g and T_i, similar to results on thiol-acrylate LCEs from previous research.[17,21,27,28]

Our LCE demonstrated a greater ability to absorb energy dissipation than TangoBlack when strain energy density was measured. Comparing Lattice A structures, the LCE structure had up to 27 times greater strain energy density than the TangoBlack structure. Our results also showed that changing lattice design allows the energy dissipation to be tuned in our LCE lattices. Both Lattices B and C had at least 3 times more energy dissipation than Lattice A in every direction of loading. Other research groups have explored the dissipation properties of optimized lattice geometries.[3,4,29] In these previous studies, groups investigated tailoring buckling geometries of rigid plastics, which trap energy in an elastic instability rather than dissipating energy through viscous mechanisms.

By creating arbitrary-shaped devices with high resolution lattice structures, we show that we can dictate and control mechanical properties of energy absorbing devices across length scales—from the chemistry of the LC resin (meso), to the architecture of the lattice used (micro), and finally the ultimate geometry of a structure to create bespoke devices for a given application (macro). Changing lattice geometries changed stress responses under different strain rates. From this information, we can derive which geometries may be better for specific applications and devices. We further show that we can incorporate different structures, geometries, and details into a singular device, such as the CU Denver coin in Figure 1a, which consists of solid walls, dense lattices, and arbitrary lettering—features all accurately reproduced in the physical print. Key to our high-quality prints is the bespoke LC resin developed for this work which is based on the two-stage thiol-acrylate LCE chemistry published by Yakacki et al. in 2015.[21] Here, the use of an organic solvent, toluene, ensures a low-viscosity resin which is printable at room temperature.

This study is the first to explore 3D-printed LCE structures for applications in tailoring energy dissipation via various length scales and to compare them to a traditional elastomer. Other studies of 3D-printed LCEs have largely focused on tailoring actuation behaviors through alignment of the mesogens during printing. For example, using DIW of LC oligomers Kotikian et al. used print speeds to increase order and thermal actuation and Ambulo et al. programmed +1 topological defects which thermal switched between Gaussian and non-Gaussian geometries.[19] While Tabrizi et al. used DLP 3D printing of a mesogenic resin to create molecularly aligned thermally and UV-responsive actuating devices, the diacrylate-based resins used to create densely cross-linked and likely glassy LC network structures as opposed to the soft elastomeric materials developed and printed here.[30]

In this study, we have not explored the influence of monodomain LCE alignment on dissipation. While employing monodomains would allow further control over device mechanical behaviors, the additional equipment required—for example, the strong magnets, additional motors, and heating elements used by Tabrizi et al.—to induce monodomain alignment during printing would vastly increase the complexity of the printing process. Given the polydomain LCE studied here offers significantly improved performance over conventional resins, we do not think an added complexity required for printing monodomains is yet justified.[30] Unlike the resins described by Tabrizi et al., our resin can be printed using commercially available DLP and SLA printers, thus allowing the rapid development of commercial devices.[30] Going forward, we anticipate the performance of dissipative LCE lattice devices could be further enhanced and tailored through buckling geometries that are predominantly stretching the members, rather than bending, and by using negative Poisson's ratio architectures.[31] For example, the high level of detail achievable with DLP 3D printing would allow for gussets to be designed to strengthen structures. Another aspect of DLP-printed lattices we did not explore was how print orientation affects the mechanical responses of the printed structures. We defined the x-, y-, and z-axis based on the orientation of the STL in our slicing software and tested the structures on each axis. Further studies could work to quantify the impact of changing the orientation of a part during printing.

This study is a step toward realizing applications for dissipative devices made with LCEs by combining the inherent material properties of LCEs and the design freedoms offered by DLP printing. The highly rate-dependent mechanical properties of our DLP-printable LC resin has great potential in biomedical devices. A recent study by Shaha et al. showed that LCEs can mimic the modulus and tan δ of biological tissues, such as the intervertebral disc.[32] Our proof-of-concept DLP-printed porous lattice LCE spinal cage device illustrates this potential (Figure 2). More widely, 3D-printed LCE lattices could be applied to shock- and vibration-absorbing devices for electronics or machinery. For instance, small devices placed in small spaces available within mobile phones could reduce the risk of screen cracks when dropped.

**ADVANCED
SCIENCE NEWS**

www.advancedsciencenews.com

**ADVANCED
MATERIALS**

www.advmat.de

Highly detailed and complex LCE structures, ranging in size from $6.5 \times 6.5 \times 3.2$ to $15.5 \times 15.5 \times 25$ mm^3, were 3D printed on a custom DLP printer with a printing resolution of 1024×768 pixels, pixel size of image of 156 μm, and layer heights ranging from 10 to 100 μm. These structures demonstrate the versatility of the custom LCE resin under various print settings for DLP printing as well as a new method of manufacturing bulk LCE structures. Structures, such as a lotus flower, were printed to show the high level of resolution achievable, while other structures, such as the lattices, were printed to show that complex features can be achieved. A porous lattice spinal cage was 3D printed on an Original Prusa SL1 (Prusa Research, Prague, Czech Republic) to show that our techniques outlined in this article can be scaled up and used to manufacture structures for practical applications. Lattice structures were used to examine energy dissipation properties of LCEs compared to common, commercially available elastomers, such as TangoBlack. LCE structures showed high degrees of rate-dependence, which was 12 times more than the TangoBlack structures at the fastest testing rates. Under quasistatic testing conditions, the Tango-Black lattices showed negligible energy loss, while LCE lattices ranged from 3.00 to 4.72 J g^{-1}. Under dynamic conditions, the LCE lattices absorbed 5–27 times more energy than the TangoB-lack lattice. Lastly, LCE Lattice A had more than 5 times greater rate-dependence than TangoBlack Lattice A when loaded at the fastest rate.

Experimental Section

Further experimental details can be found in the Supporting Information.

Materials: 2,2′-(Ethylenedioxy)diethanethiol (EDDET), phenylbis(2,4,6-trimethylbenzoyl)phosphine oxide (PPO), 2,6-di-tert-butylphenol (BHT), triethylamine (TEA), Sudan I, and toluene were purchased from Sigma Aldrich. 1,10-Decanedithiol (C10) was purchased from Fisher Scientific. 1,4-Bis-[4-(3-acryloyloxypropyloxy) benzoyloxy]-2-methylbenzene (RM257) was purchased from Wilshire Technologies. TangoBlackPlus was purchased from Stratasys. Bulk samples of neoprene, nitrile, and silicone were purchased from McMaster-Carr.

LCE Resin Preparation: Two different resins were prepared: one for experimental parts and another for a concept spinal cage device. For experimental printed parts, a 1:1 wt% ratio of RM257 and toluene were added with 2 wt% BHT and heated at 100 °C. EDDET was added in a 1.1:1 mol% ratio of mesogen to dithiol functional groups to achieve an acrylate-capped oligomer. Again 2 wt% PPO and 0.005 wt% Sudan I were added to the solution. The solution was mixed and then heated at 100 °C for 2 h. For the spinal cage, a 4:1 mol% ratio of C10 to EDDET functional groups was used to promote polymer crystallinity in the printed part. The rest of the method was identical to what was used for the experimental printed parts.

DLP Printing: For experimental printed parts, LCE and TangoBlack resins were printed at room temperature using a custom DLP 3D printer described and used in previous works by the Ge research group.[25] For the spinal cage, the LCE resin was printed at room temperature using a Prusa Research Original Prusa SL1 DLP 3D printer.

Uniaxially Compression Tests: Compressive stress–strain tests were performed using a TA Instruments ElectroForce 3200. Lattice LCE and TangoBlack structures with dimensions ≈$9 \times 9 \times 9$ mm^3 were tested. Structures were tested on each axis, such that the z-axis corresponded to the print direction and the x- and y-axes were determined from the orientation of the STL in the 2D image slicing software. The structures were tested at strain rates of 0.21, 2.2, 22, and 220% s^{-1} and their stress responses were measured to compare the rate-dependence behavior between the LCE and TangoBlack materials. Additionally, the stress responses were used to quantify energy and evaluate anisotropic responses in the lattices as well as anisotropic responses caused by print orientation.

Supporting Information

Supporting Information is available from the Wiley Online Library or from the author.

Conflict of Interest

C.M.Y. has a potential conflict of interest since he owns equity in a company that is trying to commercialize LCE products.

[1] a) Q. Chen, P. F. Cao, R. C. Advincula, *Adv. Funct. Mater.* **2018**, *28*, 1800631; b) Y. Chen, T. Li, Z. Jia, F. Scarpa, C.-W. Yao, L. Wang, *Mater. Des.* **2018**, *137*, 226.

[2] J. Mueller, J. R. Raney, K. Shea, J. A. Lewis, *Adv. Mater.* **2018**, *30*, 1705001.

[3] D. K. Patel, A. H. Sakhaei, M. Layani, B. Zhang, Q. Ge, S. Magdassi, *Adv. Mater.* **2017**, *29*, 1606000.

[4] S. R. Bates, I. R. Farrow, R. S. Trask, presented at Active and Passive Smart Structures and Integrated Systems, Las Vegas, NV, USA **2016**.

[5] T. D. Ngo, A. Kashani, G. Imbalzano, K. T. Nguyen, D. Hui, *Composites, Part B* **2018**, *143*, 172.

[6] a) O. Weeger, N. Boddeti, S.-K. Yeung, S. Kaijima, M. Dunn, *Addit. Manuf.* **2019**, *25*, 39; b) M. Kajtaz, A. Subic, *Materials in Sports Equipment*, Elsevier, Amsterdam, The Netherlands **2019**, p. 161; c) M. E. Prévôt, S. Ustunel, E. Hegmann, *Materials* **2018**, *11*, 377; d) M. Prévôt, H. Andro, S. Alexander, S. Ustunel, C. Zhu, Z. Nikolov, S. Rafferty, M. Brannum, B. Kinsel, L. Korley, *Soft Matter* **2018**, *14*, 354.

[7] H. V. Alizadeh, M. G. Fanton, A. G. Domel, G. Grant, D. B. Camarillo, arXiv:1910.07722, **2019**.

**ADVANCED
SCIENCE NEWS**
www.advancedsciencenews.com

**ADVANCED
MATERIALS**
www.advmat.de

[8] a) I. Gibson, M. F. Ashby, *Proc. R. Soc. London, Ser. A* **1982**, *382*, 43; b) E. B. Duoss, T. H. Weisgraber, K. Hearon, C. Zhu, W. Small IV, T. R. Metz, J. J. Vericella, H. D. Barth, J. D. Kuntz, R. S. Maxwell, *Adv. Funct. Mater.* **2014**, *24*, 4905.

[9] S. Shan, S. H. Kang, J. R. Raney, P. Wang, L. Fang, F. Candido, J. A. Lewis, K. Bertoldi, *Adv. Mater.* **2015**, *27*, 4296.

[10] S. Babaee, J. Shim, J. C. Weaver, E. R. Chen, N. Patel, K. Bertoldi, *Adv. Mater.* **2013**, *25*, 5044.

[11] a) A. Clausen, F. Wang, J. S. Jensen, O. Sigmund, J. A. Lewis, *Adv. Mater.* **2015**, *27*, 5523; b) O. Duncan, T. Shepherd, C. Moroney, L. Foster, P. D. Venkatraman, K. Winwood, T. Allen, A. Alderson, *Appl. Sci.* **2018**, *8*, 941.

[12] a) D. Broer, G. P. Crawford, S. Zumer, *Cross-Linked Crystal-line Systems: From Rigid Polymer Networks to Elastomers*, CRC Press, Boca Raton, FL, USA **2011**; b) W. H. De Jeu, *Liquid Crystal Elastomers: Materials and Applications*, Vol. *250*, Springer, Berlin, Germany **2012**; c) M. Warner, E. M. Terentjev, *Liquid Crystal Elastomers*, Vol. *120*, Oxford University Press, Oxford, UK **2007**.

[13] S. W. Ula, N. A. Traugutt, R. H. Volpe, R. R. Patel, K. Yu, C. M. Yakacki, *Liq. Cryst. Rev.* **2018**, *6*, 78.

[14] a) A. Kotikian, C. McMahan, E. C. Davidson, J. M. Muhammad, R. D. Weeks, C. Daraio, J. A. Lewis, *Sci. Robot.* **2019**, *4*, eaax7044; b) S. Schuhladen, F. Preller, R. Rix, S. Petsch, R. Zentel, H. Zappe, *Adv. Mater.* **2014**, *26*, 7247; c) H. Zeng, P. Wasylczyk, D. S. Wiersma, A. Priimagi, *Adv. Mater.* **2018**, *30*, 1703554.

[15] T. H. Ware, M. E. McConney, J. J. Wie, V. P. Tondiglia, T. J. White, *Science* **2015**, *347*, 982.

[16] a) S. Clarke, A. Hotta, A. Tajbakhsh, E. Terentjev, *Phys. Rev. E* **2001**, *64*, 061702; b) T. H. Ware, Z. P. Perry, C. M. Middleton, S. T. Iacono, T. J. White, *ACS Macro Lett.* **2015**, *4*, 942; c) T. Ohzono, M. O. Saed, E. M. Terentjev, *Adv. Mater.* **2019**, *31*, 1902642; d) D. R. Merkel, R. K. Shaha, C. M. Yakacki, C. P. Frick, *Polymer* **2019**, *166*, 148; e) D. Mistry, S. D. Connell, S. L. Mickthwaite, P. B. Morgan, J. H. Clamp, H. F. Gleeson, *Nat. Commun.* **2018**, *9*, 5095.

[17] M. O. Saed, A. H. Torbati, C. A. Starr, R. Visvanathan, N. A. Clark, C. M. Yakacki, *J. Polym. Sci., Part B: Polym. Phys.* **2017**, *55*, 157.

[18] R. S. Kularatne, H. Kim, J. M. Boothby, T. H. Ware, *J. Polym. Sci., Part B: Polym. Phys.* **2017**, *55*, 395.

[19] a) C. P. Ambulo, J. J. Burroughs, J. M. Boothby, H. Kim, M. R. Shankar, T. H. Ware, *ACS Appl. Mater. Interfaces* **2017**, *9*,

37332; b) A. Kotikian, R. L. Truby, J. W. Boley, T. J. White, J. A. Lewis, *Adv. Mater.* **2018**, *30*, 1706164.

[20] a) M. López-Valdeolivas, D. Liu, D. J. Broer, C. Sánchez-Somolinos, *Macromol. Rapid Commun.* **2018**, *39*, 1700710; b) R. H. Volpe, D. Mistry, V. V. Patel, R. R. Patel, C. M. Yakacki, *Adv. Healthcare Mater.* **2020**, *9*, e1901136.

[21] C. Yakacki, M. Saed, D. Nair, T. Gong, S. Reed, C. Bowman, *RSC Adv.* **2015**, *5*, 18997.

[22] K. Kowsari, S. Akbari, D. Wang, N. X. Fang, Q. Ge, *3D Print. Addit. Manuf.* **2018**, *5*, 185.

[23] X. Zheng, J. Deotte, M. P. Alonso, G. R. Farquar, T. H. Weisgraber, S. Gemberling, H. Lee, N. Fang, C. M. Spadaccini, *Rev. Sci. Instrum.* **2012**, *83*, 125001.

[24] a) G. A. Appuhamillage, N. Chartrain, V. Meenakshisundaram, K. D. Feller, C. B. Williams, T. E. Long, *Ind. Eng. Chem. Res.* **2019**, *58*, 15109; b) R. Liska, M. Schuster, R. Inführ, C. Turecek, C. Fritscher, B. Seidl, V. Schmidt, L. Kuna, A. Haase, F. Varga, *J. Coat. Technol. Res.* **2007**, *4*, 505.

[25] Q. Ge, A. H. Sakhaei, H. Lee, C. K. Dunn, N. X. Fang, M. L. Dunn, *Sci. Rep.* **2016**, *6*, 31110.

[26] A. Azoug, V. Vasconcellos, J. Dooling, M. Saed, C. Yakacki, T. Nguyen, *Polymer* **2016**, *98*, 165.

[27] a) N. Traugutt, R. Volpe, M. Bollinger, M. O. Saed, A. Torbati, K. Yu, N. Dadivanyan, C. Yakacki, *Soft Matter* **2017**, *13*, 7013; b) D. R. Merkel, N. A. Traugutt, R. Visvanathan, C. M. Yakacki, C. P. Frick, *Soft Matter* **2018**, *14*, 6024.

[28] M. O. Saed, R. H. Volpe, N. A. Traugutt, R. Visvanathan, N. A. Clark, C. M. Yakacki, *Soft Matter* **2017**, *13*, 7537.

[29] a) H. G. Hosseinabadi, R. Bagheri, L. A. Gray, V. Altstädt, K. Drechsler, *Polym. Test.* **2017**, *63*, 163; b) C. Ge, L. Priyadarshini, D. Cormier, L. Pan, J. Tuber, *Packag. Technol. Sci.* **2018**, *31*, 361; c) H. Y. Sarvestani, A. Akbarzadeh, H. Niknam, K. Hermenean, *Compos. Struct.* **2018**, *200*, 886.

[30] M. Tabrizi, T. H. Ware, M. R. Shankar, *ACS Appl. Mater. Interfaces* **2019**, *11*, 28236.

[31] J. Mueller, K. H. Matlack, K. Shea, C. Daraio, *Adv. Theory Simul.* **2019**, *2*, 1900081.

[32] R. K. Shaha, D. R. Merkel, M. P. Anderson, E. J. Devereaux, R. R. Patel, A. H. Torbati, N. Willett, C. M. Yakacki, C. P. Frick, *J. Mech. Behav. Biomed. Mater.* **2020**, *107*, 103757.